Alloying route to tailor giant magnetic anisotropy in transition-metal nanowires

N. N. Negulyaev,[1] J. Dorantes-Dávila,[2] L. Niebergall,[1] L. Juárez-Reyes,[3] G. M. Pastor,[3] and V. S. Stepanyuk[1]
[1]*Max-Planck-Institut für Mikrostrukturphysik, Weinberg 2, D-06120 Halle, Germany*
[2]*Instituto de Física, Universidad Autónoma de San Luis Potosí, 78000 San Luis Potosí, Mexico*
[3]*Institut für Theoretische Physik, Universität Kassel, Heinrich Plett Straße 40, D-34132 Kassel, Germany*
(Received 30 January 2013; published 20 February 2013)

First-principles theoretical investigations of one-dimensional ordered 3*d*-5*d* alloys reveal magnetic anisotropy energies ΔE, which are extraordinary high for transition-metal nanostructures. The results show that ΔE of Pt-X and Ir-X wires with $X \equiv$ Ti–Ni strongly oscillates as a function 3*d*-band filling showing both giant values (e.g., $\Delta E = 25$, 58, and 57 meV/atom for Pt-Ni, Ir-Cr, and Ir-Ni) as well as modest enhancements (e.g., $\Delta E = 2.3$ and 6.5 meV/atom for Pt-Cr and Pt-Fe). The robustness of the results with respect to strain and relaxation is demonstrated. The microscopic mechanisms behind the trends in ΔE are analyzed from a local perspective.

DOI: 10.1103/PhysRevB.87.054425 PACS number(s): 75.75.−c, 71.15.−m, 75.30.Gw, 75.50.Cc

I. INTRODUCTION

The magnetism of one-dimensional (1D) systems is not only fascinating from a fundamental perspective but also very promising for technological applications such as recording media, memory devices, and spintronics.[1,2] Consequently, the experimental and theoretical research activities in this field have been most intense over the past years.[2–4] One of the properties of central importance in these materials is the magnetic anisotropy energy (MAE) which defines the low-energy orientation of the magnetization $\vec{M}$ (easy axis) as well as the stability of $\vec{M}$ with respect to external fields, electric currents, and temperature-induced fluctuations. Large MAEs per atom are intensively sought, for example, in order to achieve device miniaturization and enhanced storage density. Symmetry and dimensionality are known to play a crucial role in this context, particularly for itinerant-electron transition-metal (TM) compounds. Indeed, 3*d*-TM wires develop large, stable spin and orbital magnetic moments together with MAEs that are orders of magnitude larger than in the corresponding solids.[5,6] Nevertheless, despite this remarkable enhancement, the absolute values of the MAEs remain relatively small due to the weak spin-orbit (SO) coupling in the 3*d* elements. Stronger SO interactions, as found in the heavier 5*d* TMs, should in principle lead to larger anisotropies.[7–9] However, the nanostructures consisting solely of 5*d* elements adopt either nonmagnetic ground states or weakly magnetic states, which depend critically on strain and relaxation.[7,8] These complementary behaviors suggest that appropriate combinations of 3*d* and 5*d* elements would allow us to merge the large moments and magnetic stability of 3*d* TMs, the strong SO coupling of 5*d* TMs, and the extremely low-dimensional environment of 1D wires in order to achieve unprecedentedly large and robust MAEs. The relevance of the problem is backed up by the numerous experimental possibilities of synthesizing 1D materials, for example, by scanning-tunneling-microscope (STM) atom manipulation,[10] by exploiting auto-organization on vicinal and flat surfaces,[4,11] and in nearly freestanding geometries between substrate and STM tips[12] or at break junctions.[13–16] It is the main goal of this paper to report theoretical investigations showing under which circumstances and to what extent such exceptional enhancements of the MAE are possible.

Although the potential advantages of alloying highly polarizable 5*d* TMs with 3*d* elements in 1D systems can be understood straightforwardly, the subject also raises a number challenging open questions. In fact, all main alloy parameters, such as composition, concentration, and chemical order, are expected to affect the magnetic behavior in a nontrivial way. One would like to understand, for example, the dependence of the magnetic order as a function of composition and the consequences of 3*d*-5*d* charge transfers on the local moments. Equally intriguing is the role of structural relaxation and strain on orbital magnetism and SO energies. Furthermore, the magnetic proximity effects on the 5*d* atoms, which are induced by the weakly magnetic or antiferromagnetic elements at the beginning of the 3*d* series, should be very different form those induced by the strongly ferromagnetic elements at the series end. This opens plenty of new possibilities of tuning the MAE as a function of the alloying element. It is therefore quite remarkable that only very few theoretical investigations of orbital magnetism and magnetic anisotropy of one-dimensional alloys are available at present. Among them, one should mention the density-functional study of Wang *et al.*[17] who reported very large MAEs in freestanding Fe-5*d* monoatomic wires which are significantly reduced upon encapsulation in carbon nanotubes. Progress in this multifaceted field certainly requires quantitative investigations based on quantum theory. But in addition, it is also important to analyze and correlate the different electronic and magnetic properties (for example, the energy as a function of the magnetization direction, the spin and orbital magnetic moments, and the underlying electronic structure) in order to shed light on the mechanisms responsible for the magnetic anisotropy of 1D alloys. In this way a lasting contribution to knowledge-based material design can be achieved.

In the following we consider ordered alloy wires having equal concentrations, which maximize the 3*d*-5*d* magnetic proximity effects. Furthermore, we focus on the freestanding geometry, where the most extreme low-dimensional phenomena are expected. The effects of strain and relaxations resulting from interactions at substrates and break junction are explored by varying the interatomic distances and the shape of the wire. The role of 3*d*-band filling and the possibility of tuning the MAE that it offers are investigated in Pt-X and Ir-X wires by varying $X \equiv$ Ti–Ni systematically across the 3*d* series. Pt and

Ir are particularly relevant examples of 5*d* metals due to their high spin polarizability and strong SO coupling.

II. COMPUTATIONAL METHOD

The calculations have been performed by using the Vienna *ab initio* simulation package (VASP) which implements Hohenberg-Kohn-Sham's density-functional theory on a periodic supercell and allows fully-self-consistent structural relaxations.[18] The VASP solves the spin-polarized Kohn-Sham equations in an augmented plane-wave basis set, taking into account the core electrons within the projector augmented wave (PAW) method.[19] This is an efficient frozen-core all-electron approach that allows one to incorporate the proper nodes of the Kohn-Sham orbitals in the core region and the resulting effects on the electronic structure, total energy, and interatomic forces. Exchange and correlation (XC) effects are treated within Perdew and Wang's generalized-gradient approximation (GGA).[20] Both ferromagnetic (FM) and antiferromagnetic (AF) alignments of the magnetic moments in neighboring two-atom unit cells are considered. This, together with the freedom of the 3*d* and 5*d* moment alignment within each cell, allows us to take into account FM and AF super-exchange-like couplings of the 3*d* moments mediated by the intermediate 5*d* atom and vice versa [see the inset of Fig. 1(a)]. Notice that other magnetic states such as spin-density waves or noncollinear arrangements may occur by manipulating the interatomic distances or by depositing chains on polarizable substrates.[21–24] The robustness of our results has been explicitly checked by performing comparative calculations using the Ceperly-Alder XC functional[25] and the full-potential WIEN2K method.[26] Furthermore, a number of tests have been performed in order to assess the numerical accuracy of the calculations. We have increased our standard calculation parameters—namely, cutoff energy $E_{\max} = 268$ eV, supercell size perpendicular to the wire $a = 12$ Å, and k-point mesh $n_k = 1 \times 1 \times 61$—to $E_{\max} = 500$ eV, $a = 14$ Å and $n_k = 1 \times 1 \times 91$. Although this increases the computation time by a factor 20, the results do not change significantly. For example, the equilibrium bond length of a pure Pt wire changes from 2.383 to 2.381 Å and the total-energy differences involved in the MAE per atom change by 0.1 meV or less. These small changes in the numerical results have no influence on our physical conclusions. We have also verified that the total energy is nearly independent of the energy level smearing σ, provided that it is not too large ($1 \leqslant \sigma \leqslant 50$ meV). One concludes that our choice of computational parameters provides the necessary accuracy at a reasonable computational cost.

III. RESULTS AND DISCUSSION

Figure 1(a) shows the *ab initio* calculated MAE $\Delta E = E_x - E_z$ of FM and AF Pt-3*d* linear wires at their corresponding equilibrium distance r_0, where E_δ stands for the total energy per atom when the magnetization $\vec{M}$ points along the axis δ. The coordinate system and the magnetic orders are illustrated in the insets of Fig. 1. Both FM and AF chains show strong even-odd-like oscillations of ΔE as a function of the 3*d* element. A similar behavior has been previously observed

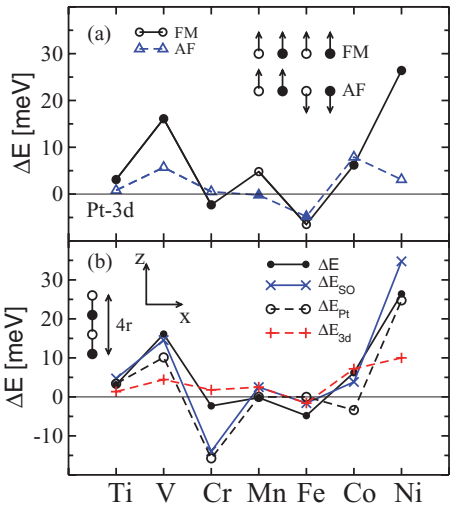

FIG. 1. (Color online) (a) *Ab initio* MAE per atom $\Delta E = E_x - E_z$ of linear Pt-3*d* wires having FM (circles, full lines) or AF (triangles, broken lines) orders at their equilibrium NN distances r_0. The solid symbols indicate the ground-state magnetic order. Positive (negative) values of ΔE correspond to an in-line (perpendicular) easy axis as illustrated in the inset. (b) Comparison between the ground-state *ab initio* ΔE, the model spin-orbit anisotropy energy $\Delta E_{\rm SO}$, and the element-specific local MAEs ΔE_{3d} and $\Delta E_{\rm Pt}$.

in pure 3*d* and 4*d* wires as a function of *d*-band filling.[5,8] Moreover, one observes that ΔE is in general larger for FM order than for AF order. As we shall see, this is related to the full quenching of the Pt moments in the AF configuration in which the Pt atoms are framed by antiparallel NN 3*d* moments. For some alloy wires, for example Pt-V and Pt-Ni, remarkably large values of the MAE are found ($\Delta E \simeq 20$ meV) which contrast with the nearly vanishing MAE of pure Pt wires at their equilibrium distance.[7] In other cases, ΔE is quite small, of the same order as the MAE of pure 3*d* wires.[6] For instance, $|\Delta E| \leqslant 2$ meV for Pt-Cr and Pt-Mn. Therefore, achieving giant MAEs is far from obvious. The nontrivial dependence of MAE on 3*d* doping element defies easy generalizations. It is interesting to notice that the calculated MAE of Pt-Co wires is quantitatively comparable to previous experimental results of Co monoatomic chains deposited on a Pt substrate.[4] This indicates that the MAE obtained for freestanding alloy wires can also provide useful insights on more complex situations, provided that the local environments are alike, for instance, similar low coordination numbers and type of neighbors.

In order to obtain a qualitative microscopic understanding of the trends in the MAE of 3*d*-5*d* wires it is useful to focus on the changes in the z component of the intra-atomic SO energy

$$E_{\rm SO} = \frac{1}{N}\sum_{\alpha} \xi_\alpha (L_{\alpha\uparrow} - L_{\alpha\downarrow})/2, \qquad (1)$$

where ξ_α refers to SO coupling constant at atom α, $L_{\alpha\sigma}$ to the z component of the spin-resolved local orbital moment, and N to the number of atoms. Equation (1) neglects the transversal or spin-flip off-diagonal terms of the SO coupling, which are proportional to $(\hat{L}^+_\alpha \hat{S}^-_\alpha + \hat{L}^-_\alpha \hat{S}^+_\alpha)$, as well as the contributions to ΔE due to the anisotropy of the kinetic and

Coulomb energies. The former terms dominate in the limit of large exchange splitting and saturated moments, where the SO energy is mainly given by the coupling between electrons having the same spin (minority electrons above half-band filling).[27,28] However, the later terms can be crucial if important redistributions of the spin-polarized density occur upon rotating $\vec{M}$. This is manifested by an anisotropy of the spin moments. Numerical stability often precludes computing these contributions self-consistently within first-principles theories.[29–31] Fully self-consistent studies of MAE have been performed in the framework of tight-binding theory.[5]

Assuming for simplicity that the anisotropy of the orbital moments $\Delta L = L_x - L_z$ is dominated by the majority-spin (minority-spin) electrons below (above) half d-band filling, the anisotropy of $E_{\rm SO}$ can be written as

$$\Delta E_{\rm SO} = \frac{1}{N}\sum_{\alpha}\Delta E_{\alpha} \simeq \frac{1}{N}\sum_{\alpha}(\pm\xi_{\alpha}/2)\Delta L_{\alpha}, \qquad (2)$$

where the positive (negative) sign applies to Ti–Mn (Fe–Ni and Pt). This simple approximation is an alloy extension of the proportionality relation between ΔE and ΔL derived by Bruno for homogeneous systems with saturated spin moments.[32] $\Delta E_{\rm SO}$ is calculated by using the local orbital moments within the Wigner-Seitz spheres and the atomic values for ξ_{3d} and ξ_{5d}.[32] A local perspective to the MAE is provided by the element-resolved anisotropy energies ΔE_{3d} and ΔE_{5d} at the $3d$ and $5d$ atoms. It should be however noted that the perspective adopted in Eqs. (1) and (2) neglects the off-site transitions due to the SO interactions. Although these contributions are generally expected to be much weaker than the usual intra-atomic terms, they need not be completely negligible, particularly in strongly hybridized itinerant electrons systems.[33]

In Fig. 1(b) ΔE, $\Delta E_{\rm SO}$, ΔE_{3d}, and $\Delta E_{\rm Pt}$ of Pt-$3d$ wires are compared by taking their corresponding values of the local orbital moments shown in Table I. One observes that the model $\Delta E_{\rm SO}$ reproduces qualitatively well the variations of ΔE as a function of $3d$ element. Except for Pt-Cr wires, even the quantitative values are quite accurate. This validates the assumed dominant role of the diagonal part of the spin-orbit interactions, as compared to the transversal terms and the kinetic plus Coulomb anisotropy energies. Concerning the local components, one observes that the Pt contribution is responsible for the even-odd-like oscillations, while the $3d$ contribution, besides being quantitatively weaker in general, depends more smoothly on the $3d$ element. In most cases, the ΔE_{3d} and $\Delta E_{\rm Pt}$ have the same sign and thus favor the same easy axis. However, in Pt-Cr and Pt-Co wires the $3d$ and Pt contributions are competing. In the case of Pt-Co wires, these competing contributions result in a rather small value of $\Delta E_{\rm SO}$. In fact, $\frac{1}{2}(-\xi_{\rm Co}/2\Delta L_{\rm Co}) = 7.2$ meV while $\frac{1}{2}(-\xi_{\rm Pt}/2\Delta L_{\rm Pt}) = -3.4$ meV yielding $\Delta E_{\rm SO} = 3.8$ meV. In contrast, in Pt-Ni wire $\frac{1}{2}(-\xi_{\rm Ni}/2\Delta L_{\rm Ni}) = 10$ meV and $\frac{1}{2}(-\xi_{\rm Pt}/2\Delta L_{\rm Pt}) = 26.4$ meV, which add up resulting in a remarkably large value of $\Delta E_{\rm SO}$. Moreover, in AF Pt-Mn and Pt-Fe wires $\Delta E_{\rm Pt}$ vanishes so that the $3d$ term dominates. One concludes that none of the local ΔE_{α} *alone* is able to account for the trends in ΔE. It is therefore inaccurate to assume that the anisotropy of $3d$-$5d$ alloy wires originates essentially at the heavier $5d$ atoms. Instead, we find important mutual proximity effects: The $3d$ atoms polarize Pt and thus trigger large values of $\Delta E_{\rm Pt}$, and the Pt atoms enhance ΔE_{3d} beyond the levels typically found in pure $3d$ wires.[5,6]

Table I shows results for the local spin and orbital moments μ_z and L_z, corresponding to the in-line magnetization direction, and μ_x and L_x for the radial magnetization direction. The different magnetic orders are illustrated in the inset of Fig. 1(a). Concerning the ground-state configuration, we find that the Pt and $3d$ moments are antiparallel to each other at the beginning of the series (Ti, V, and Cr) while they are parallel at the series end (Co and Ni). In all these cases the magnetic moments are the same in all the unit cells, despite the antiparallel coupling between NNs. These configurations are thus FM from the perspective of the Pt-$3d$ unit cells. Remarkably, Pt-Mn and Pt-Fe wires show an AF coupling between neighboring Pt-$3d$ cells [see inset of Fig. 1(a) and Table I]. In these cases the Pt atoms are framed by two $3d$ NNs carrying antiparallel moments. As a result, the Pt moments vanish. These trends in the magnetic order are not affected by reasonable variations of the interatomic distances r around the equilibrium value r_0. In connection with the magnetic order it is interesting to point out that there is a significant charge transfer from the $3d$ to the $5d$ orbitals (typically 0.5 electrons). This brings in particular Fe closer to half d-band filling and probably favors the observed AF order in Pt-Fe wires.

TABLE I. Spin and orbital moments in Pt-$3d$ wires at their equilibrium interatomic distances: μ_z and L_z correspond to the in-line magnetization direction, while μ_x and L_x correspond to a perpendicular radial direction. The results are given in $\mu_{\rm B}$ ($\mu_{\alpha} = 2S_{\alpha}$) for the ferromagnetic (FM) and antiferromagnetic (AF) configurations (see Fig. 1). The corresponding MAEs $\Delta E = E_x - E_z$ are given in meV/atom.

	Ti	V	Cr	Mn	Fe	Co	Ni
μ_z/μ_x (Pt, FM)	−0.15/ −0.14	−0.24/ −0.22	−0.18/ −0.20	0.32/0.23	0.66/0.64	0.64/0.66	0.60/0.47
L_z/L_x (Pt, FM)	−0.11/ −0.08	−0.21/ −0.12	−0.06/ −0.20	0.01/ −0.12	0.28/0.23	0.25/0.28	0.38/0.16
μ_z/μ_x ($3d$, FM)	1.51/1.51	2.62/2.61	3.63/3.63	4.27/4.26	3.45/3.45	2.27/2.32	1.00/0.96
L_z/L_x($3d$, FM)	−0.30/0.06	−0.63/0.08	−0.04/0.14	−0.10/0.16	−0.16/0.21	0.47/0.15	0.44/0.04
μ_z/μ_x (Pt, AF)	0.00/0.00	0.00/0.00	0.00/0.00	0.00/0.00	0.00/0.00	0.00/0.00	0.00/0.00
L_z/L_x (Pt, AF)	0.00/0.00	0.00/0.00	0.00/0.00	0.00/0.00	0.00/0.00	0.00/0.00	0.00/0.00
μ_z/μ_x ($3d$, AF)	0.95/0.94	2.06/2.05	3.36/3.38	4.02/4.02	3.26/3.26	2.10/2.09	0.47/0.00
L_z/L_x ($3d$, AF)	−0.20/0.04	−0.49/0.17	−0.23/0.50	−0.07/0.13	0.12/0.20	0.74/ −0.16	0.30/ −0.00
ΔE (FM)	3.1	16.1	−2.3	4.8	−6.5	6.2	26.4
ΔE (AF)	0.8	5.7	0.5	−0.2	−4.8	7.9	3.1

The local $3d$ spin moments increase first from $2S_{\mathrm{Ti}} = 1.51\mu_{\mathrm{B}}$ to $2S_{\mathrm{Mn}} = 4.27\mu_{\mathrm{B}}$, by approximately $1\mu_{\mathrm{B}}$ per additional $3d$ electron, and then decrease from $2S_{\mathrm{Fe}} = 3.45\mu_{\mathrm{B}}$ to $2S_{\mathrm{Ni}} = 1.0\mu_{\mathrm{B}}$. On the other side, the Pt spin moments are systematically larger at the end of the $3d$ series (e.g., $2S_{\mathrm{Pt}} = 0.60$–0.66 in Pt-Co and Pt-Ni wires) than for small d-band filling [e.g., $2S_{\mathrm{Pt}} = -(0.15$–$0.24)$ for Pt-Ti, Pt-V, and Pt-Cr wires]. In addition, one observes that the orbital moments $L_{\mathrm{Pt}} \simeq (0.2$–$0.4)\mu_{\mathrm{B}}$ and $L_{3d} \simeq (0.4$–$0.6)\mu_{\mathrm{B}}$ are quite important, yielding large total moments $2S_\alpha + L_\alpha$. Notice in particular the large orbital moment $L_{\mathrm{Ni}} \simeq 0.4\mu_{\mathrm{B}}$ in Pt-Ni wires, which correlates with its large MAE (see Table I).

In the ground state the coupling between spin and orbital local moments follows Hund's third rule for all considered Pt-$3d$ wires, if the direction of the magnetization is along the wire, regardless of the actual magnetic order. In fact, only in one case, namely, the Pt-Cr wire whose easy axis is perpendicular to the wire, we find a quantitatively small violation of the third Hund rule (see Table I). For $3d$ elements below half-band filling (Ti, V, and Cr) the spin and orbital moments are antiparallel, while in Mn, Fe, Co, and Ni atoms S and L are parallel. Pt atoms always shows parallel S and L. Only in some energetically unfavorable magnetic configurations (for example, in AF Co-Pt wires) one finds a violation of Hund's third rule. Moreover, one observes that the easy-magnetization axis corresponds in general to the direction yielding the maximum total orbital moment $L_{\mathrm{Pt}} + L_{3d}$. This simple trend holds for both FM and AF wires, provided that the local orbital moments are not too small ($L_{\mathrm{Pt}}, L_{3d} > 0.1\mu_{\mathrm{B}}$).

The orbital moments of the different Pt-$3d$ wires can be qualitatively correlated with the corresponding electronic structures. In Fig. 2 the spin-polarized local densities of states (LDOS) of Pt-Ti, Pt-Cr, and Pt-Ni wires are shown as representative examples. The d states may be classified, according to their spatial symmetry, in the subspaces $\Delta_0 = \{d_{z^2}\}$, $\Delta_1 = \{d_{xz}, d_{yz}\}$, and $\Delta_2 = \{d_{xy}, d_{x^2-y^2}\}$, which are invariant in the absence of SOC.[6,8] Figure 2 shows how these bands are split by the SO interactions. The degree of occupation of the Δ_2 states explains the formation of the orbital moment L_z along the in-line direction z.[8] If the Δ_2 band is fully occupied, L_z is very small. This holds for Pt in the Pt-Ti wire ($L_{z,\mathrm{Pt}} = 0.12\mu_{\mathrm{B}}$) and for Pt and Cr in the Pt-Cr wire ($L_{z,\mathrm{Pt}} = 0.07\mu_{\mathrm{B}}$ and $L_{z,\mathrm{Cr}} = 0.04\mu_{\mathrm{B}}$; see Fig. 2). On the other hand, if the Δ_2 LDOS is not fully occupied—particularly when it exhibits peaks at the Fermi energy E_F—one obtains large values of L_z.[6] This is for example the case of Ti in the Pt-Ti wire ($|L_{z,\mathrm{Ti}}| = 0.3\mu_{\mathrm{B}}$) and most notably at the Ni and Pt atoms in the Pt-Ni wire ($L_{z,\mathrm{Ni}} = 0.44\mu_{\mathrm{B}}$ and $L_{z,\mathrm{Pt}} = 0.38\mu_{\mathrm{B}}$). For the off-line magnetization direction one generally observes smaller values of L_x, due to the partial occupation of mixed Δ_1-Δ_2 states.[8] Moreover, we find that L_x is not completely quenched only if there are Δ_1 states at E_F. Otherwise it is zero. Finally, it is interesting to mention that the electronic structure and orbital moments L_{Pt} in the Pt-Cr wire are very similar to those found in Pd monoatomic wires. The Δ_2 states, which lie well below E_F, yield $L_z \simeq 0$, while the larger values of L_x are developed by the Δ_1 states at E_F.[34] The present analysis of the LDOS is not only relevant for Pt-$3d$ wires in the ultimate low-dimensional limit of weak wire-environment interactions. It also shows that the magnetoanisotropic effects found in freestanding wires should be preserved in the presence of weak interactions with the environment or support, provided that the nature of the electronic states close to E_F is preserved.

In Fig. 3 results for the MAE of Ir-$3d$ wires are shown, while the local spin and orbital moments are given in Table II. The effects of $3d$-$5d$ alloying are even stronger than in Pt-based wires, particularly concerning the spin and orbital polarization of Ir and the resulting exceptionally large MAEs (e.g., $\Delta E \simeq 60$ meV for Ir-Cr and Ir-Ni wires). The main trends in the magnetoanisotropic behavior may be summarized as follows: (i) The MAE of both FM and AF wires oscillates as a function of the $3d$ element, being maximal for Ir-Cr, minimal for Ir-Fe, and increasing again in Ir-Ni. As in Pt-$3d$ wires, the MAE is in general larger for FM than for AF order. (ii) The calculated $\Delta E \simeq 60$ meV of Ir-Cr and Ir-Ni wires at or near the NN equilibrium distances is quite remarkable for

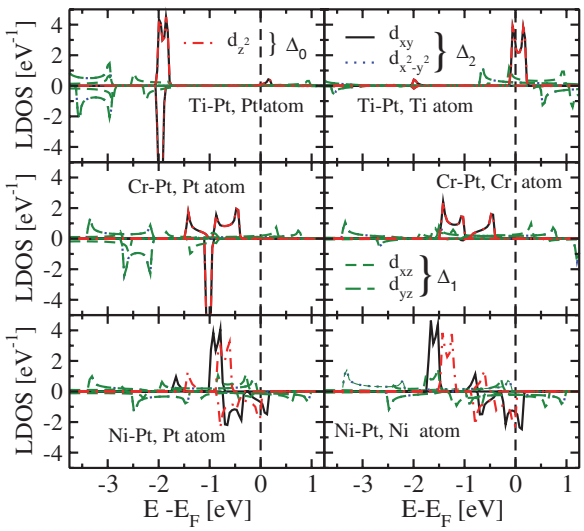

FIG. 2. (Color online) Local density of states (LDOS) of FM Pt-Ti, Pt-Cr, and Pt-Ni wires at their equilibrium NN distances. Results are given for the projections on the d-electron irreducible subspaces Δ_0, Δ_1, and Δ_2 of the Pt (left) and $3d$ (right) atoms.

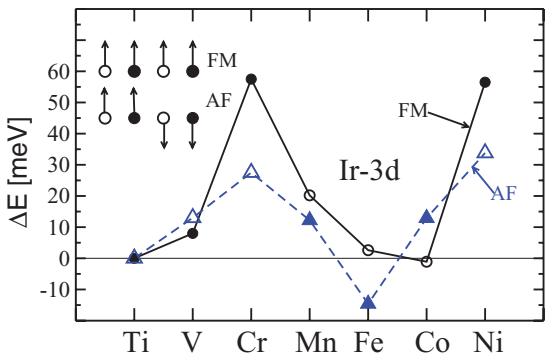

FIG. 3. (Color online) (a) *Ab initio* MAE per atom $\Delta E = E_x - E_z$ of linear Ir-$3d$ wires having FM (circles, full lines) or AF (triangles, broken lines) orders at their equilibrium NN distances r_0. The solid symbols indicate the ground-state magnetic order (see the inset). Positive (negative) values of ΔE correspond to an in-line (perpendicular) easy axis.

TABLE II. Spin and orbital moments in Ir-3d wires at their equilibrium interatomic distances: μ_z and L_z correspond to the in-line magnetization direction, while μ_x and L_x correspond to a perpendicular radial direction. The results are given in μ_B ($\mu_\alpha = 2S_\alpha$) for the ferromagnetic (FM) and antiferromagnetic (AF) configurations (see Fig. 3). The corresponding MAEs $\Delta E = E_x - E_z$ are given in meV/atom.

	Ti	V	Cr	Mn	Fe	Co	Ni
μ_z/μ_x (Ir, FM)	0.00/0.00	−0.65/ −0.59	−0.80/ −0.64	1.18/0.32	1.01/0.66	1.11/0.86	1.39/0.81
L_z/L_x (Ir, FM)	0.00/0.00	−0.52/ −0.14	−0.99/ −0.25	1.44/ −0.10	0.80/ −0.06	0.81/0.04	1.22/0.18
μ_z/μ_x (3d, FM)	0.00/0.00	2.20/2.20	3.35/3.31	4.15/4.06	2.92/2.82	1.69/1.66	0.87/0.54
L_z/L_x (3d, FM)	0.00/0.00	−0.19/0.06	−0.19/0.11	−0.03/0.17	−0.32/0.33	−0.11/0.23	0.23/0.11
μ_z/μ_x (Ir, AF)	0.00/0.00	0.00/0.00	0.00/0.00	0.98/0.07	0.00/0.00	0.86/0.00	1.16/0.69
L_z/L_x (Ir, AF)	0.00/0.00	0.00/0.00	0.00/0.00	1.60/0.03	0.00/0.00	0.78/0.00	1.45/0.44
μ_z/μ_x (3d, AF)	0.00/0.00	1.33/1.20	2.46/2.47	3.80/3.80	2.95/2.93	1.75/1.76	0.00/0.00
L_z/L_x (3d, AF)	0.00/0.00	−0.75/0.05	−0.35/0.15	−0.06/0.19	−0.43/0.25	0.38/0.18	0.00/0.00
ΔE (FM)	0.0	8.0	57.5	20.2	2.6	−1.1	56.5
ΔE (AF)	0.0	13.0	27.0	12.2	−14.6	12.9	33.8

the MAE in TM nanostructures. In contrast, the MAE of Ir-Fe and Ir-Co wires is very modest or vanishing. (iii) Ir-Ti wires are found to be paramagnetic at their equilibrium distance r_0. Wires having 3d TMs below half-band filling (V and Cr) show an antiparallel alignment of the Ir magnetic moments relative to the 3d moments (see Table II). In these cases all Ir-3d unit cells are magnetically equivalent (FM intercell correlations). In contrast, the 3d elements in the middle of the series, at and above half-band filling (Mn, Fe, and Co) yield a parallel alignment of the moments within the Ir-3d unit cells and an AF order between neighboring Ir-3d pairs. The energy differences between the FM and AF configurations is typically 60–160 meV/atom. At the end of the 3d series, Ir-Ni wires show FM order both within and between Ir-Ni cells (see Table II). Similarly strong dependence of the MAE on the d-band filling have already been observed in thin-film studies.[35,36] (iv) The model SO anisotropy energy ΔE_{SO} yields the correct sign of ΔE and thus reproduces the *ab initio* easy axis, since the latter is the direction yielding the largest orbital moments per atom. (v) The local anisotropy energy ΔE_{Ir} dominates over ΔE_{3d} thus controlling the dependence of the MAE on the 3d element. As in Pt-based wires, ΔE_{3d} depends rather smoothly on the 3d element. (vi) It is interesting to observe that the MAE of Ir-Fe freestanding chains is quantitatively comparable to the results of previous calculations for Fe chains deposited on an Ir substrate.[37,38] This suggests, as already observed for Pt-Co chains, that similar coordination numbers and alloy environments often lead to similar enhancements of the MAE. (vii) In contrast to Pt-3d wires, the simple SO anisotropy model is not applicable quantitatively, since in Ir-3d wires very important redistributions of the spin- and orbital-polarized density occur upon rotating $\vec{M}$. As a result, strong anisotropies of the spin moments take place, which are related to the strong hybridizations between the 3d and 5d elements.[27,28,39] For example, in Ir-Mn, $2S_{Mn} = 0.98\mu_B$ and $L_{Mn} = 1.60\mu_B$ when $\vec{M}$ is in-line, while $2S_{Mn} = 0.07\mu_B$ and $L_{Mn} = 0.03\mu_B$ when $\vec{M}$ is perpendicular to the wire (see Table II). Under such circumstances it is important to take into account the spin-flip terms of the SO coupling and the changes in the kinetic and Coulomb energies upon rotating $\vec{M}$. These contributions tend to compensate ΔE_{SO} and thus reduce the actual MAE. Consequently, the simple model for ΔE_{SO} given by Eq. (2) often yields a large overestimation of ΔE, by an order of magnitude in Ir-Mn. Despite this limitation, the phenomenological model has been very useful in order to reveal the importance of this subtle many-body effect on the MAE of 1D alloy wires.

The robustness of our results with respect to changes in the local environment and wire-substrate interactions can be explored by varying the NN distance r and the shape of the wires. In Fig. 4 the MAE of Pt-Ni and Ir-Cr wires is given as a function of r. Results for pure Pt and Ir wires are included for the sake of comparison. In agreement with previous studies,[7] we find an extremely weak or vanishing ΔE in pure Pt wires having r smaller or equal to their equilibrium distance

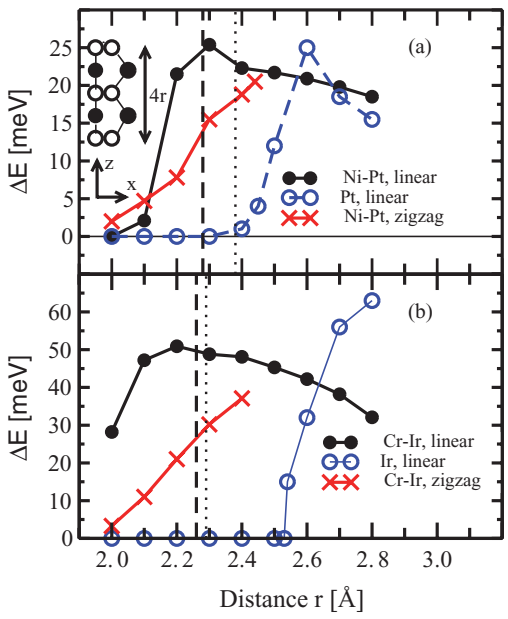

FIG. 4. (Color online) MAE per atom $\Delta E = E_x - E_z$ of (a) Pt-Ni and (b) Ir-Cr wires as a function of the NN distance r. Results are given for linear (dots) and zigzag (crosses) alloy wires, as well as for pure linear 5d wires (open circles). The magnetization directions x and z are illustrated in the inset. The dotted (dashed) vertical lines indicate the equilibrium NN distance r_0 in pure 5d (alloy 3d-5d) linear wires.

TABLE III. Stability and equilibrium bond lengths of Pt-3*d* and Ir-3*d* wires: Segregation energy $E_S = (E_{3d5d} - E_{3d} - E_{5d})/2$, equilibrium bond length r_0 in the ferromagnetic (FM) and antiferromagnetic (AF) configurations, and exchange energy $E_{\rm AF} - E_{\rm FM}$. The radii of the atomic 3*d* shells r_{3d} are reproduced from Ref. 40. Energies are given in meV/atom and distances in Å.

	Ti	V	Cr	Mn	Fe	Co	Ni
Pt-3*d*							
E_S	−940	−550	−490	−660	−420	−170	−100
r_0(FM)	2.34	2.32	2.33	2.38	2.32	2.30	2.28
r_0(AF)	2.34	2.30	2.33	2.34	2.30	2.28	2.27
$E_{\rm AF} - E_{\rm FM}$	62	216	188	−62	−46	18	42
Ir-3*d*							
E_S	−990	−700	−240	−190	−170	70	140
r_0(FM)	2.20	2.22	2.27	2.38	2.25	2.21	2.26
r_0(AF)	2.20	2.18	2.20	2.33	2.21	2.20	2.23
$E_{\rm AF} - E_{\rm FM}$	0	146	231	−48	−158	−52	20
r_{3d}	1.64	1.42	1.30	1.21	1.15	1.09	1.03

$r_0 = 2.38$ Å. Only for $r > r_0$ one finds a rapid increase of ΔE as the Pt moments set in, reaching a maximal $\Delta E = 25$ meV for about 8% bond-length expansion. The situation changes drastically upon doping. For example, in Pt-Ni wires one obtains $\Delta E \simeq 25$ meV at and even below the already smaller equilibrium distance $r_0 = 2.28$ Å. Very large values of ΔE are found within the relatively wide range 2.2 Å $\leqslant r \leqslant$ 2.8 Å. The consequences of 3*d* doping are even more dramatic in Ir-based wires. Pure Ir wires are paramagnetic for $r \leqslant 2.53$ Å, i.e., unless they are expanded more than 10% beyond equilibrium ($r_0 = 2.28$ Å). Alloying with Cr atoms induces very important spin and orbital moments ($2S_{\rm Ir} = 0.8\mu_{\rm B}$ and $L_{\rm Ir} = 1.0\mu_{\rm B}$) and, consequently, a colossal enhancement of $\Delta E \simeq 50$ meV at the equilibrium distance $r_0 = 2.28$ Å. The effect is so withstanding that it persists even for r as small as 2 Å [see Fig. 4(b)]. Finally, we have also investigated zigzag Pt-Ni and Ir-Cr wires in order to assess the effects of geometry changes on the MAE. In fact, for any monoatomic wire there is a critical unit cell length $2r_c$ along the wire below which, in the absence of lateral constraints, the linear chain becomes less stable than the zigzag configuration.[6,9] For example, for Pt-Ni one obtains $r_c = 2.45$ Å, and for Ir-Cr $r_c = 2.41$ Å. As shown in Fig. 4, the MAE of zigzag wires decreases linearly with decreasing wire length. However, a remarkable enhancement of ΔE remains, provided that r is not too far from r_0. For example, $\Delta E \simeq 15$ meV for zigzag Pt-Ni and $\Delta E \simeq 30$ meV for zigzag Cr-Ir with $r \simeq r_0$ (see Fig. 4). These results quantify the robustness of the alloying route to giant MAE.

In view of artificially made wires, it is interesting to explore whether the 3*d* species favor the formation of alloys with the 5*d* atoms, or whether strong tendencies to segregation should be expected. For a given interatomic distance r, a measure of the alloy stability in free chains is given by the energy difference $E_S = (E_{3d5d} - E_{3d} - E_{5d})/2$, where E_{3d}, E_{5d}, and E_{3d5d} are the total ground-state energies per atom of pure 3*d*, 5*d*, and mixed 3*d*-5*d* wires at their corresponding equilibrium distances. Results for E_S are shown in Table III. One observes that Pt-3*d* wires and most of the Ir-3*d* wires tend to form alloys, since $E_S < 0$ at the equilibrium distance $r = r_0$ (see the second and third rows of Table III). Only in Ir-Co and Ir-Ni wires segregation is more stable ($E_S > 0$). The absolute value of E_S generally decreases as one follows the 3*d* series from Ti to Ni. This can be explained in terms of the radius r_{3d} of the 3*d* shell, which monotonically decreases from Ti to Ni (see the first row in Table III). Taking into account[40] that r_{3d}(Pt) $\simeq r_{3d}$(Ir) $\simeq r_{3d}$(Ti) one concludes that the smaller the value of r_{3d} is, the larger is the mismatch between 3*d* and 5*d* atoms. Consequently, at the end of the 3*d* series segregation is energetically more favorable.

IV. CONCLUSION

In conclusion, a first-principles investigation of 3*d*-5*d* 1D alloys revealed exceptionally large values of the MAE ΔE, particularly in Pt-Ni, Ir-Cr, and Ir-Ni wires. The development of very high ΔE is found to be far more elusive than *a priori* expected. The changes in ΔE as a function of the 3*d* element have been qualitatively correlated to the details of the electronic structure close to the Fermi energy. The theoretical discussion has been complemented with an analysis from a local perspective by identifying the element-specific SO contributions to ΔE. While in Pt-3*d* wires the MAE can be traced back to a SO coupling mechanism, in Ir-3*d* wires one observes more complex many-body effects, which involve strong redistributions of the spin- and orbital-polarized density as a function of the direction of the magnetization $\vec{M}$. This indicates that the anisotropy of the kinetic and Coulomb energies is quantitatively very important. The robustness of the results with respect to strain and bond-length relaxations has been quantified. TM alloy wires thus emerge as an extremely promising field of fundamental and technological research from both experimental and theoretical viewpoints.

ACKNOWLEDGMENTS

This work was supported in part by CONACyT-Mexico (Grant No. 62292), the Deutsche Forschungsgemeinschaft, the COST Action MP0903, and the DAAD-CONACyT research program PROALMEX. Computer resources were provided by IT Service Center of the University of Kassel. We also thank J. Renteria and J. C. Sánchez for technical support.

[1]C. H. Marrows and B. J. Hickey, Phil. Trans. R. Soc. A **369**, 3027 (2011); A. A. Khajetoorians, J. Wiebe, B. Chilian, and R. Wiesendanger, Science **332**, 1062 (2011).
[2]S. S. P. Parkin, M. Hayashi, and L. Thomas, Science **320**, 190 (2008).
[3]D. A. Allwood, G. Xiong, C. C. Faulkner, D. Atkinson, D. Petit, and R. P. Cowburn, Science **309**, 1688 (2005); P. Xu, K. Xia, C. Z. Gu, L. Tang, H. F. Yang, and J. J. Li, Nat. Nanotechnol. **3**, 97 (2008).
[4]P. Gambardella, A. Dallmeyer, K. Maiti, M. C. Malagoli, W. Eberhardt, K. Kern, and C. Carbone, Nature (London) **416**, 301 (2002); P. Gambardella, S. Rusponi, M. Veronese, S. S. Dhesi, C. Grazioli, A. Dallmeyer, I. Cabria, R. Zeller, P. H. Dederichs, K. Kern, C. Carbone, and H. Brune, Science **300**, 1130 (2003).
[5]J. Dorantes-Dávila and G. M. Pastor, Phys. Rev. Lett. **81**, 208 (1998).
[6]J. C. Tung and G. Y. Guo, Phys. Rev. B **76**, 094413 (2007).
[7]A. Smogunov, A. DalCorso, A. Delin, R. Weht, and E. Tosatti, Nat. Nanotechnol. **3**, 22 (2008).
[8]Y. Mokrousov, G. Bihlmayer, S. Heinze, and S. Blügel, Phys. Rev. Lett. **96**, 147201 (2006); A. Thiess, Y. Mokrousov, and S. Heinze, Phys. Rev. B **81**, 054433 (2010).
[9]J. C. Tung and G. Y. Guo, Phys. Rev. B **81**, 094422 (2010).
[10]N. N. Negulyaev, V. S. Stepanyuk, L. Niebergall, P. Bruno, W. Hergert, J. Repp, K.-H. Rieder, and G. Meyer, Phys. Rev. Lett. **101**, 226601 (2008).
[11]O. V. Stepanyuk, N. N. Negulyaev, P. A. Ignatiev, M. Przybylski, W. Hergert, A. M. Saletsky, and J. Kirschner, Phys. Rev. B **79**, 155410 (2009).
[12]H. Ohnishi, Y. Kondo, and K. Takayanagi, Nature (London) **395**, 780 (1998); V. Rodrigues, J. Bettini, P. C. Silva, and D. Ugarte, Phys. Rev. Lett. **91**, 096801 (2003).
[13]J. Bettini, F. Sato, P. Z. Coura, S. O. Dantas, D. S. Galvão, and D. Ugarte, Nat. Nanotechnol. **1**, 182 (2006).
[14]N. Agraït, A. Levy Yeyati, and J. M. van Ruitenbeek, Phys. Rep. **377**, 81 (2003), and references therein.
[15]J. Velev, R. F. Sabirianov, S. S. Jaswal, and E. Y. Tsymbal, Phys. Rev. Lett. **94**, 127203 (2005); A. Sokolov, C. Zhang, E. Y. Tsymbal, and J. Redepenning, Nat. Nanotechnol. **2**, 171 (2007).
[16]A. DalCorso, A. Smogunov, and E. Tosatti, Phys. Rev. B **74**, 045429 (2006); Y. Miura, R. Mazzarello, A. DalCorso, A. Smogunov, and E. Tosatti, *ibid*. **78**, 205412 (2008); P. Lucignano, R. Mazzarello, A. Smogunov, M. Fabrizio, and E. Tosatti, Nat. Mater. **8**, 563 (2009).
[17]J. Wang, C. Jo, and R. Wu, Appl. Phys. Lett. **92**, 032507 (2008).
[18]G. Kresse and J. Hafner, Phys. Rev. B **47**, 558 (1993); G. Kresse and J. Furthmüller, *ibid*. **54**, 11169 (1996).
[19]P. E. Blöchl, Phys. Rev. B **50**, 17953 (1994); G. Kresse and D. Joubert, Phys. Rev. **59**, 1758 (1999).
[20]J. P. Perdew and Y. Wang, Phys. Rev. B **45**, 13244 (1992).
[21]M. Zelený, M. Šob, and J. Hafner, Phys. Rev. B **80**, 144414 (2009).
[22]M. Saubanère, M. Tanveer, P. Ruiz-Díaz, and G. M. Pastor, Phys. Status Solidi B **247**, 2610 (2010).
[23]J. C. Tung and G. Y. Guo, Phys. Rev. B **83**, 144403 (2011).
[24]F. Schubert, Y. Mokrousov, P. Ferriani, and S. Heinze, Phys. Rev. B **83**, 165442 (2011).
[25]D. M. Ceperley and B. J. Alder, Phys. Rev. Lett. **45**, 566 (1980).
[26]K. Schwarz and P. Blaha, Comput. Mater. Sci. **28**, 259 (2003).
[27]G. van der Laan, J. Phys.: Condens. Matter **10**, 3239 (1998).
[28]D. S. Wang, R. Wu, and A. J. Freeman, Phys. Rev. B **47**, 14932 (1993).
[29]A. R. Mackintosh and O. K. Andersen, in *Electrons at the Fermi Surface*, edited by M. Springford (Cambridge University Press, Cambridge, 1980); M. Weinert, R. E. Watson, and J. W. Davenport, Phys. Rev. B **32**, 2115 (1985).
[30]D. S. Wang, R. Wu, and A. J. Freeman, Phys. Rev. Lett. **70**, 869 (1993).
[31]P. Błoński and J. Hafner, Phys. Rev. B **79**, 224418 (2009).
[32]P. Bruno, in *Magnetismus von Festkörpern und Grenzflächen*, edited by P. H. Dederichs, P. Grünberg, and W. Zinn (KFA, Jülich, 1993), Chap. 24.
[33]In order to explore this matter, we have considered the anisotropy of the total orbital moment $\Delta L_{\mathrm{T}} = \Delta L_{5d} + \Delta L_{3d}$, calculated within the Wigner-Seitz spheres of the unit cell, as a possible means of interpreting the *ab initio* results for ΔE. It turns out that the relation $\Delta E = \xi_{\mathrm{eff}} \Delta L_{\mathrm{T}}$ is not able to reproduce the first-principles trends as a function of the $3d$ element. Even the sign of ΔE is often missed. The main reason for this is that the $3d$ and Pt (or Ir) values of the element-specific ΔL_{α}, and the corresponding contributions to the MAE, often have opposite signs. This competition between contrasting local contributions cannot be described just by $\Delta L_{\mathrm{T}} = \sum_{\alpha} \Delta L_{\alpha}$. A simple analysis in terms of ΔL_{T} is further complicated by the fact that the sign of the spin-orbit coupling ξ_{α} changes below and above $3d$ half-band filling.
[34]A. Delin, E. Tosatti, and R. Weht, Phys. Rev. Lett. **92**, 057201 (2004).
[35]Š. Pick and H. Dreyssé, Phys. Rev. B **46**, 5802 (1992).
[36]J. Dorantes-Dávila and G. M. Pastor, Phys. Rev. Lett. **77**, 4450 (1996).
[37]R. Mazzarello and E. Tosatti, Phys. Rev. B **79**, 134402 (2009).
[38]Y. Mokrousov, A. Thiess, and S. Heinze, Phys. Rev. B **80**, 195420 (2009).
[39]I. V. Solovyev, P. H. Dederichs, and I. Mertig, Phys. Rev. B **52**, 13419 (1995).
[40]W. A. Harrison and S. Froyen, Phys. Rev. B **21**, 3214 (1980).